TÜBİTAK

Turkish Journal of Chemistry

http://journals.tubitak.gov.tr/chem/

Research Article

Turk J Chem
(2018) 42: 941 – 957
© TÜBİTAK
doi:10.3906/kim-1707-62

Facile synthesis of IrO_2 nanoclusters and their application as catalysts in the degradation of azo dyes

Rajni LASYAL*, **Anjali GOEL**
Department of Chemistry, Kanya Gurukul Campus, Gurukul Kangri University, Haridwar, Uttarakhand, India

Received: 24.07.2017 • **Accepted/Published Online:** 30.11.2017 • **Final Version:** 03.08.2018

Abstract: A robust synthesis of iridium oxide (IrO_2) nanoclusters using methanol as a reducing agent via the chemical reduction method is reported in this article. Polyvinylpyrrolidone (PVP) and polyoxyethylene(23) lauryl ether (POLE) were used as stabilizers. The formation of IrO_2 nanoclusters was confirmed by the appearance of new absorption peak at 230 nm in UV-vis spectra. XRD and TEM were used to determine the degree of crystallinity and size of nanoclusters, respectively. Further characterization studies were carried out by FT-IR spectroscopy to investigate the coordination between IrO_2 nanoclusters and stabilizers. The size of the nanoclusters was found to be a factor of the ratio of solvent to reductant and precursor to stabilizer. It was found that PVP-stabilized IrO_2 nanoclusters are smaller in size with narrow distribution in contrast to POLE-stabilized IrO_2 nanoclusters. The catalytic activity of these nanoclusters was examined in the degradation of some azo dyes, acid orange 10 (AO 10), acid red 14 (AR 14), and acid red 26 (AR 26), in aqueous medium. PVP-stabilized IrO_2 nanoclusters are catalytically more efficient than POLE-stabilized IrO_2 nanoclusters, which was supported by the calculation of turnover frequencies. Thus, IrO_2 nanoclusters are expected to play an imperative role in the field of catalysis and environmental remediation.

Key words: IrO_2 nanoclusters, polyvinylpyrrolidone, polyoxyethylene(23) lauryl ether, turnover frequency, environmental remediation

1. Introduction

Nanoclusters of the Pt-group metals with a face-centered cubic structure (i.e. Pt, Pd, Rh, and Ir) have received particular interest in recent years because of their outstanding performance in a variety of industrially important catalytic reactions.[1] These nanoclusters have also been employed in water treatment, such as removal of hazardous dyes and other toxic organic compounds and metals from water.[2–4] It is well documented that the activity and selectivity of such nanoclusters are highly dependent on the size of these particles.[5] Among these, IrO_2 nanoclusters have a wider range of applications than traditional catalysts because of their high activity, stability, selectivity, and mild reaction conditions to produce high yield in less reaction time.[6] This has explored its potential in catalysis. The cost for preparation of IrO_2 nanoclusters is challenging in material production. Therefore, a simple method, low-cost starting materials, and other suitable parameters are the main necessities for the synthesis of IrO_2 nanoclusters. Hence, it is very important to design a synthetic method using cheap and nontoxic reagents. However, the size, morphology, stability, and properties of synthesized IrO_2 nanoclusters are also of great importance and should be taken into consideration.

*Correspondence: lasyal.rajni@gmail.com

In this paper, the synthesis of IrO_2 nanoclusters with controllable particle size and stable dispersion by a simple chemical reduction method using methanol as a reducing agent and a polymer, polyvinylpyrrolidone (PVP), and a surfactant, polyoxyethylene(23) lauryl ether (POLE), as stabilizing agents has been reported. The size of the IrO_2 nanoclusters was considerably influenced by the ratios of solvent to reductant and precursor to stabilizer. Therefore, different sizes of IrO_2 nanoclusters were obtained by varying the amount of reductant and stabilizer.

Various organic compounds such as dyes from the textile and other industries contaminate water bodies, thereby causing water pollution.[7,8] These dyes can be degraded oxidatively by the use of metal oxide nanoclusters, which act as excellent catalysts in the degradation process.[9,10] In this paper, the oxidative degradation of three azo dyes, acid orange 10 (AO 10), acid red 14 (AR 14), and acid red 26 (AR 26), by hexacyanoferrate(III), abbreviated as HCF(III), using IrO_2 nanoclusters as catalyst has been reported. Herein, the catalytic activity of synthesized PVP-stabilized IrO_2 nanoclusters and POLE-stabilized IrO_2 nanoclusters in the degradation of these dyes has also been compared by the calculation of turnover frequencies for the first time.

2. Results and discussion

2.1. UV-visible analysis

UV-vis spectroscopy is a convenient technique for monitoring the progress of metal colloid formation. As can be seen from Figures 1a and 1b, initially $IrCl_3^{3-}$ exhibits an absorption peak at 260 nm, which disappears on addition of methanol, and a new peak appears at 206 nm. This new peak gradually decreases and disappears completely after 25 min of refluxing, indicating that $IrCl_3^{3-}$ ions are completely reduced (Figures 2a and 2b). Appearance of new peak at 230 nm may be attributed to the formation of IrO_2 nanoclusters.[11]

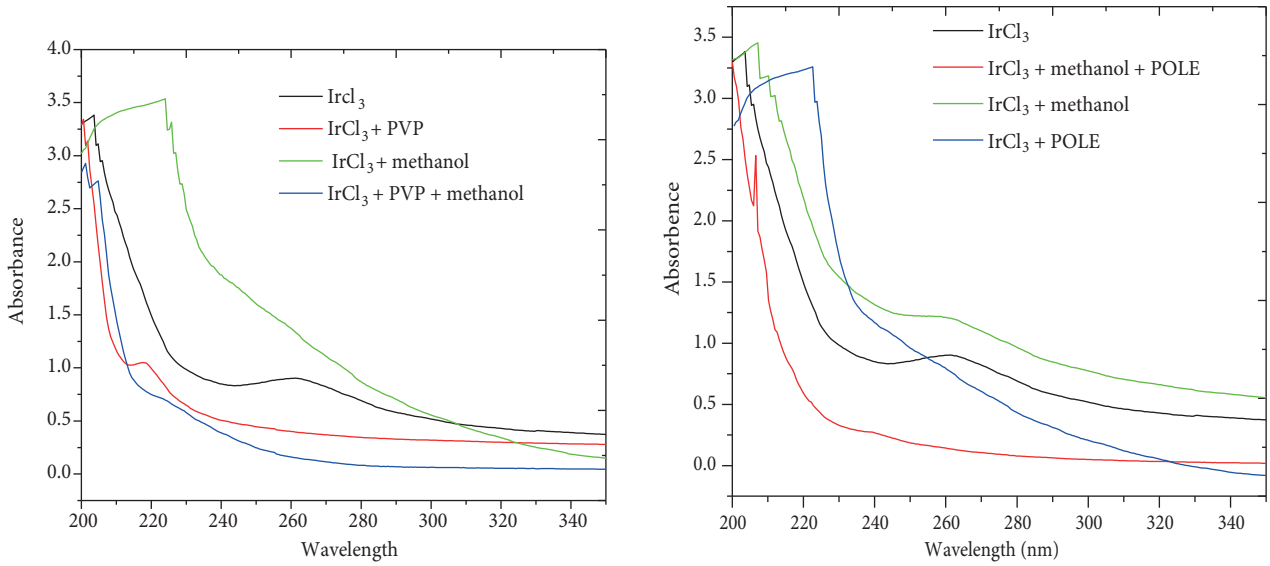

Figure 1. a. UV-vis spectra of different reactants during the formation of IrO_2 nanoclusters in PVP-$IrCl_3$-methanol-water system. b. UV-vis spectra of different reactants during the formation of IrO_2 nanoclusters in POLE-$IrCl_3$-methanol-water system.

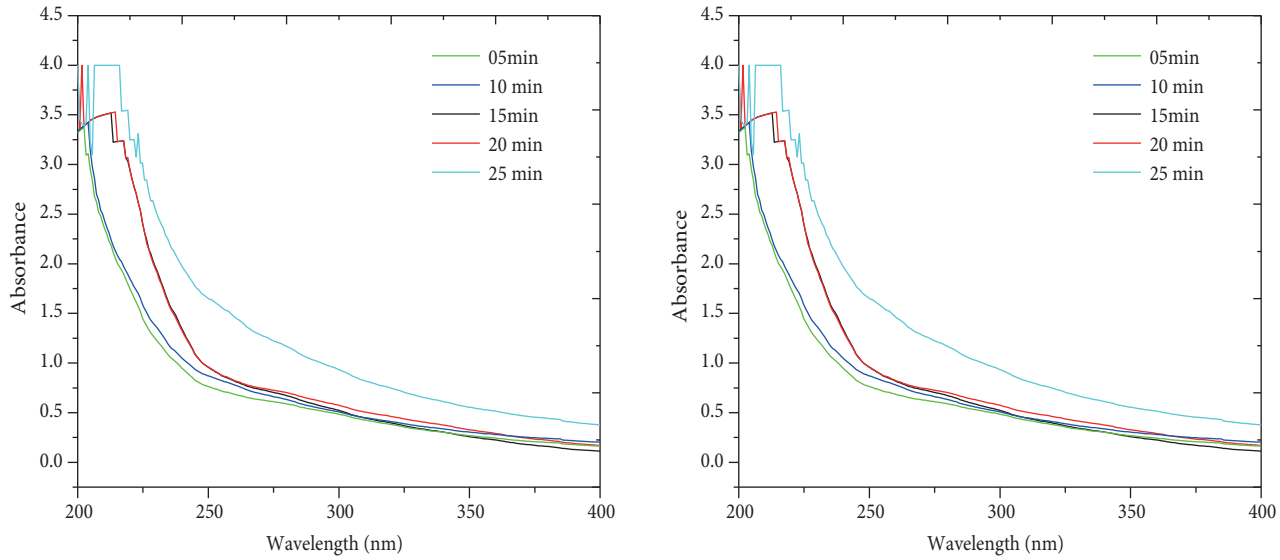

Figure 2. a. Time-dependent UV-vis spectra for the formation of PVP-stabilized IrO_2 nanoclusters. b. Time-dependent UV-vis spectra for the formation of POLE-stabilized IrO_2 nanoclusters.

2.2. XRD studies

Figures 3 and 4 show the XRD pattern of PVP-stabilized IrO_2 nanoclusters and POLE-stabilized IrO_2 nanoclusters, respectively. The XRD pattern of PVP-stabilized IrO_2 nanoclusters (Figure 3) shows two broad peaks at 2-theta of about 28° and 40◦ at reflection plane Ir(110) and Ir(200), respectively, which are characteristic of isolated IrO_2 nanoclusters. Analysis of the peaks' broadening using the Scherrer equation gives an estimate of particle diameter. Diameters of the particles calculated by the Scherrer equation are given in Table 1. The particle size ranges between 4.32 and 5.13 nm by method 'a' and between 5.16 and 5.86 nm by method 'c'. In the present work particles synthesized by method 'b', in the range of 4.12 to 4.71 nm, are smallest in size and possess the smallest range of dispersion.

Table 1. Synthesis conditions and particle size of IrO_2 nanoclusters with PVP.

Method	Solvent / reductant	Water: methanol (v/v)	$IrCl_3.xH_2O$: PVP (w/w)	NaOH (ml)	Reflux time	Approximate particle size (nm)	
						XRD	TEM
a.	Methanol	1 : 1.1	1 : 25	1 mL	2 h	4.32, 5.13	-
b.	Methanol	1 : 1.4	1 : 25	1 mL	2 h	4.12, 4.71	4.05 ± 0.25
c.	Methanol	1 : 1.9	1 : 25	1 mL	2 h	5.16, 5.86	-

Similarly, the XRD patterns of POLE-stabilized IrO_2 nanoclusters show the characteristic peaks at (110), (200), and (210) planes corresponding to 28°, 40°, and 45° on the 2-theta scale for IrO_2 nanoparticles. It can be seen from Figure 4 that in contrary to PVP-stabilized IrO_2 nanoclusters, these are larger in size, more dispersed, and crystalline in nature. Approximate particle size of the particles is represented in Table 2. For method 'a', particle size ranges from 17.26 to 43.12 nm, which decreases to 16.45 to 24.65 nm for method 'c' via 17.02 to 25.71 nm for method 'b'. Methods 'd' and 'f' have particle size in the ranges of 14.18 to 28.87 nm and 24.26 to 34.49 nm, respectively. The X-ray diffractograms of these metallic particles indicate that PVP-

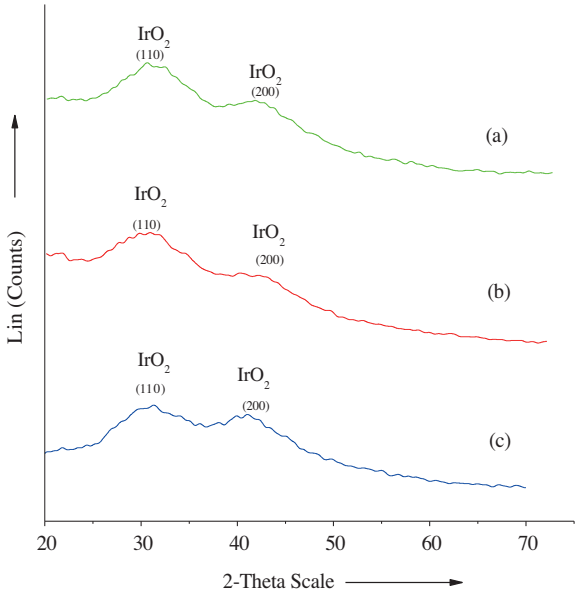

Figure 3. XRD pattern of PVP-stabilized IrO_2 nanoclusters synthesized by chemical reduction methods a, b, and c as represented in Table 1.

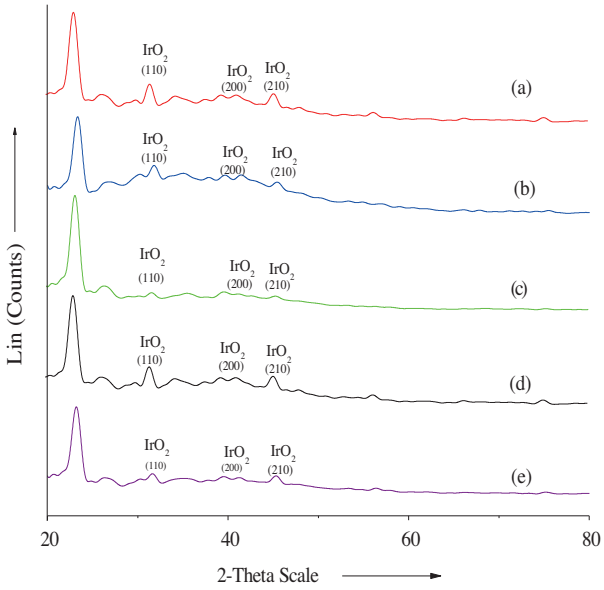

Figure 4. XRD pattern of POLE-stabilized IrO_2 nanoclusters synthesized by chemical reduction methods a, b, c, d, and f as represented in Table 2.

stabilized IrO_2 nanoclusters are amorphous with broad peaks characteristic of materials with small size, while POLE-stabilized IrO_2 nanoclusters are crystalline in nature and larger in size. It is observed that an increase in water to reductant (v/v) ratio leads to the formation of larger particles. A similar effect on the particle size was observed for POLE-stabilized IrO_2 nanoclusters (Table 2) for the water to reductant (v/v) ratio. Data presented in Table 2 for POLE-stabilized IrO_2 nanoclusters also reveal that the particle size is proportional to the precursor to stabilizer (w/w) ratio.

Table 2. Synthesis conditions and particle size of IrO_2 nanoclusters with POLE.

Method	Solvent / reductant	Water: methanol (v/v)	$IrCl_3.xH_2O$: POLE (w/w)	NaOH (ml)	Reflux time	Approximate particle size (nm)	
						XRD	TEM
a.	Methanol	1 : 1.4	1 : 37	1 mL	2 h	17.26, 23.56, 43.12,	-
b.	Methanol	1 : 1.4	1 : 25	1 mL	2 h	17.02, 18.82, 25.71	36.36 ± 1.0
c.	Methanol	1 : 1.4	1 : 18	1 mL	2 h	16.45, 18.60, 24.65	21.21 ± 1.3
d.	Methanol	1 : 1.1	1 : 18	1 mL	2 h	14.18, 16.48, 28.87	-
e.	Methanol	1 : 1.9	1 : 18	1 mL	2 h	-	25.0 ± 2.5
f.	Methanol	1 : 2.4	1 : 18	1 mL	2 h	24.2, 32.99, 34.49	45.40 ± 2.5

Comparison of data presented in Tables 1 and 2 shows that PVP-stabilized IrO_2 nanoclusters are smaller in size with a narrow range of distribution in contrast to POLE-stabilized IrO_2 nanoclusters. Under similar synthesis conditions (method 'b' in Tables 1 and 2), POLE- stabilized IrO_2 nanoclusters are nine times larger with a broader range of size distribution as compared to PVP-stabilized IrO_2 nanoclusters. Hence, from the above studies, it is evident that the size of IrO_2 nanoclusters can be tuned by controlling the amount of reductant, precursor, and stabilizer.

2.3. FT-IR studies

Comparative study of the FT-IR spectra in Figures 5a–5c for $IrCl_3$, pure PVP, and PVP-stabilized IrO_2 nanoclusters clearly illustrates the chemical interaction between IrO_2 nanoclusters and the polymeric stabilizer (PVP). It is observed that a strong band at 1687 cm^{-1} representing the amide >C=O group in PVP shifts to 1650 cm^{-1}. This shift may occur due to bond weakening as a result of the partial bond formation with surface metal atoms, which eventually passivate the surface of IrO_2 nanoclusters (Figures 5b and 5c). However, bands at 2953 and 2874 cm^{-1} corresponding to asymmetric and symmetric stretching vibrations of the C-H bond and the band at 1433 cm^{-1} that resulted from vibration of the tertiary nitrogen of PVP (Figure 5b) are not involved in the stabilization process.[12,13] Figure 5c shows the appearance of a new band at 2015 cm^{-1} attributed to IrO_2 nanoclusters and the disappearance of bands at 2353 and 2322 cm^{-1} (Figure 5a) due to Ir(III).[14]

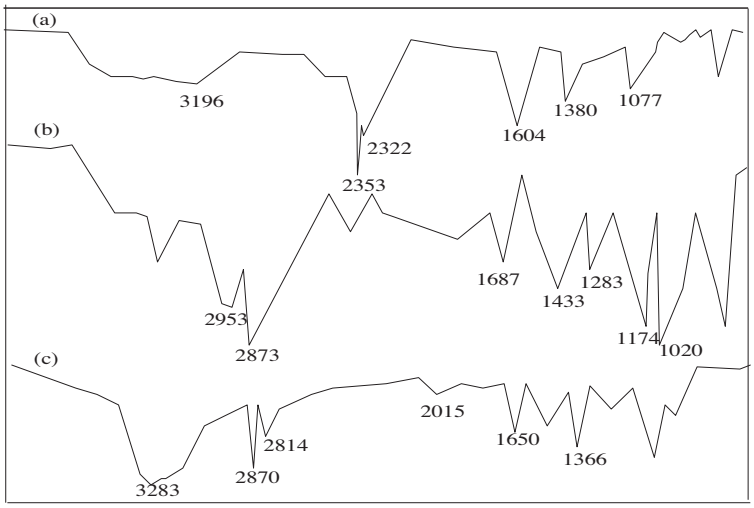

Figure 5. FT-IR spectra of (a) pure $IrCl_3$, (b) pure PVP, and (c) PVP-stabilized IrO_2 nanoclusters.

Figures 6a–6c show the IR spectra of precursor iridium, pure POLE, and IrO_2 nanoclusters, respectively. Precursor iridium shows bands at 3196, 2353, 2322, 1604, 1380, and 1077 cm^{-1} (Figure 6a). As shown in Figure 6c, bands in the region of 2353 and 2322 cm^{-1} due to Ir(III) in the precursor disappeared and a new band appeared at 2096 cm^{-1}, indicating the formation of IrO_2,[14] while bands around 1604 and 3196 cm^{-1} in the precursor show a shift towards 1639 and 3279 cm^{-1}, corresponding to bending and stretching modes of O-H groups on the catalyst surface and surface-adsorbed water.[15] The stabilizer POLE is characterized by C-O-C symmetric and asymmetric stretching at 1103 and 1240 cm^{-1} (Figure 6b), respectively, which shift towards lower frequency of 1014 cm^{-1} in the spectra of IrO_2 nanoclusters.

2.4. TEM studies

TEM images in Figure 7a show that the PVP-stabilized IrO_2 nanoclusters are separated with no agglomeration tendency. The particle size distributions obtained from TEM images are fairly narrow and the average estimated particle size is about 4.05 $\pm$ 0.25 nm. Figures 7b-7e demonstrates that POLE-stabilized IrO_2 nanoclusters have an agglomeration tendency and are larger in size as compared to PVP-stabilized IrO_2 nanoclusters. The smallest particle size for POLE-stabilized IrO_2 nanoclusters is estimated about 21.21 $\pm$ 1.3 nm with method 'c' (Figure 7c). Representative TEM micrographs show that individual iridium oxide nanoclusters are spherical in shape.

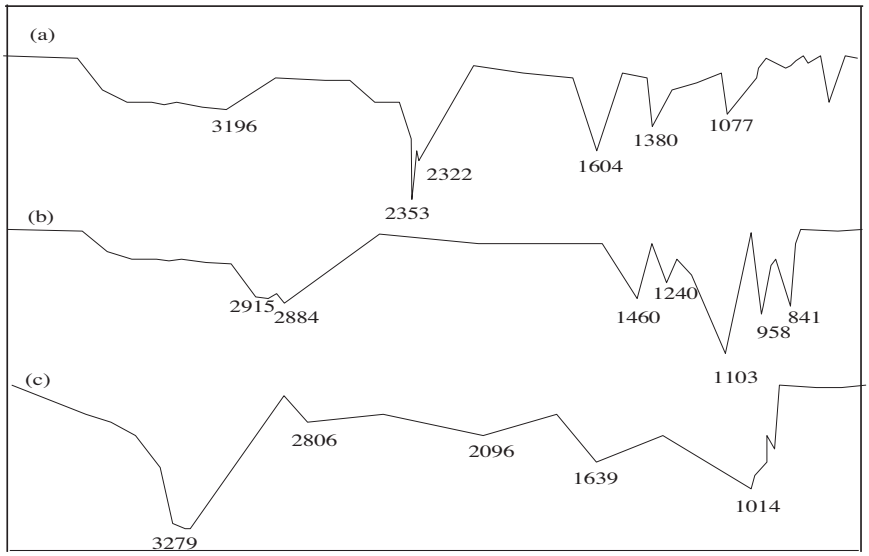

Figure 6. FT-IR spectra of (a) pure $IrCl_3$, (b) pure POLE, and (c) POLE-stabilized IrO_2 nanoclusters.

2.5. Catalytic study for the oxidation of azo dyes

The catalytic efficiency of IrO_2 nanoclusters was investigated by studying the oxidation of three azo dyes, AO 10, AR 14, and AR 26, using HCF(III) as an oxidant. Degradation of azo dyes was monitored by kinetics spectrophotometrically. Figure 8 shows the UV-vis spectrum for the degradation of AO 10. The spectrum corresponds to the disappearance of a peak at 479 nm for AO 10 and the appearance of a new peak at 241 nm suggesting the formation of a new product or products. AR 14 is characterized by maximum absorption at 515 nm attributed to the chromophore-containing azo linkage of the dye molecule in the solution. The disappearance of this band and formation of new bands at 250 and 268 nm support the degradation (Figure 9). The absorption maximum for AR 26 is observed at 507 nm. Here also, it can be seen that new bands at 245 and 273 nm suggest the degradation of the dye (Figure 10).

2.6. Comparison of catalytic activity of PVP-stabilized IrO_2 nanoclusters and POLE-stabilized IrO_2 nanoclusters

The comparison of the catalytic activity of synthesized PVP-stabilized IrO_2 nanoclusters (PVP-IrO_2-nano) and POLE-stabilized IrO_2 nanoclusters(POLE-IrO_2-nano) was conducted by carrying out the oxidation of three azo dyes, AR 10, AR 14, and AR 26, using HCF(III) as an oxidant. A graph plotted between rate vs. concentration of the catalysts shows that the rate of the PVP-IrO_2-nano-catalyzed reaction is higher than those of the reactions catalyzed by POLE- IrO_2-nano and Ir-Precursor. This reveals the highest catalytic activity of PVP- IrO_2-nano as compared to POLE-IrO_2-nano and Ir-Precursor, which is supported by the calculation of turnover frequencies (Table 3). It can also be demonstrated from Figures 11–13 that the oxidation of all three azo dyes by HCF(III) follows first-order kinetics with regard to the catalyst, i.e. Ir-Precursor / POLE-IrO_2-nano / PVP-IrO_2-nano. First-order rate constant k_1 was evaluated by the plot of log (a-x) vs. time, with slope equal to $-k_1$ / 2.303. Here, 'a' is the initial concentration of reactant and 'x' is the concentration of reactants that were converted to products at time 't'. The values of k_1 for the degradation of AO 10, AR 14, and AR 26 are summarized in Table 4. Iridium nanoparticles proved to be exceptionally efficient catalysts for the oxidation

of these azo dyes as they demonstrated an enhanced degradation rate compared to Ir-Precursor, which may be due to the large ratio of surface area to volume. Moreover, these nanoparticles can be recovered and reused, making them more economical candidates for dye degradation technologies as compared to molecular iridium.

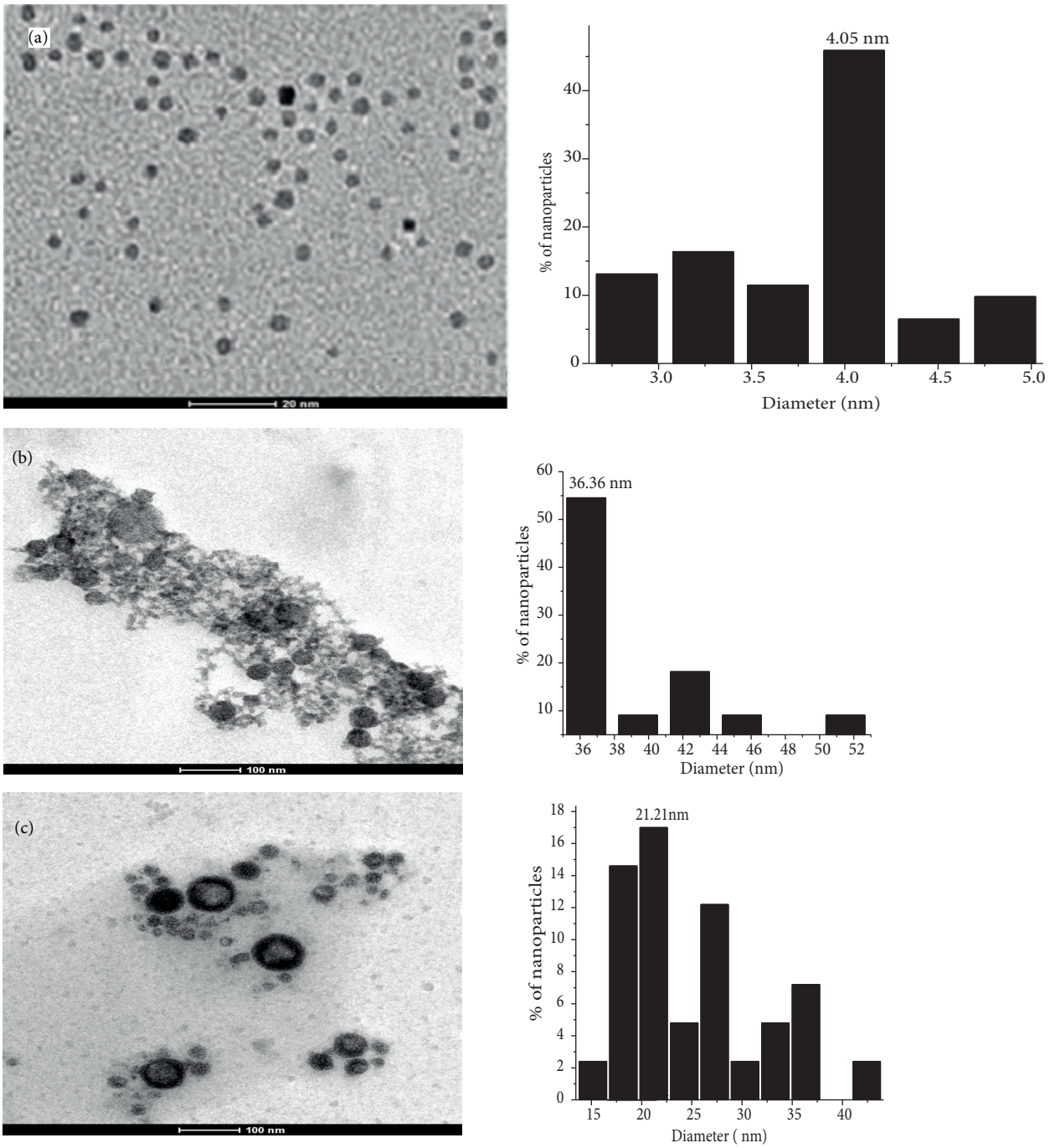

Figure 7. a. TEM micrograph and corresponding particle size distribution histogram of PVP-stabilized-IrO_2 nanoclusters (method b) b-e. TEM micrograph and corresponding particle size distribution histogram of POLE-stabilized-IrO_2 nanoclusters (methods b, c, e, and f respectively).

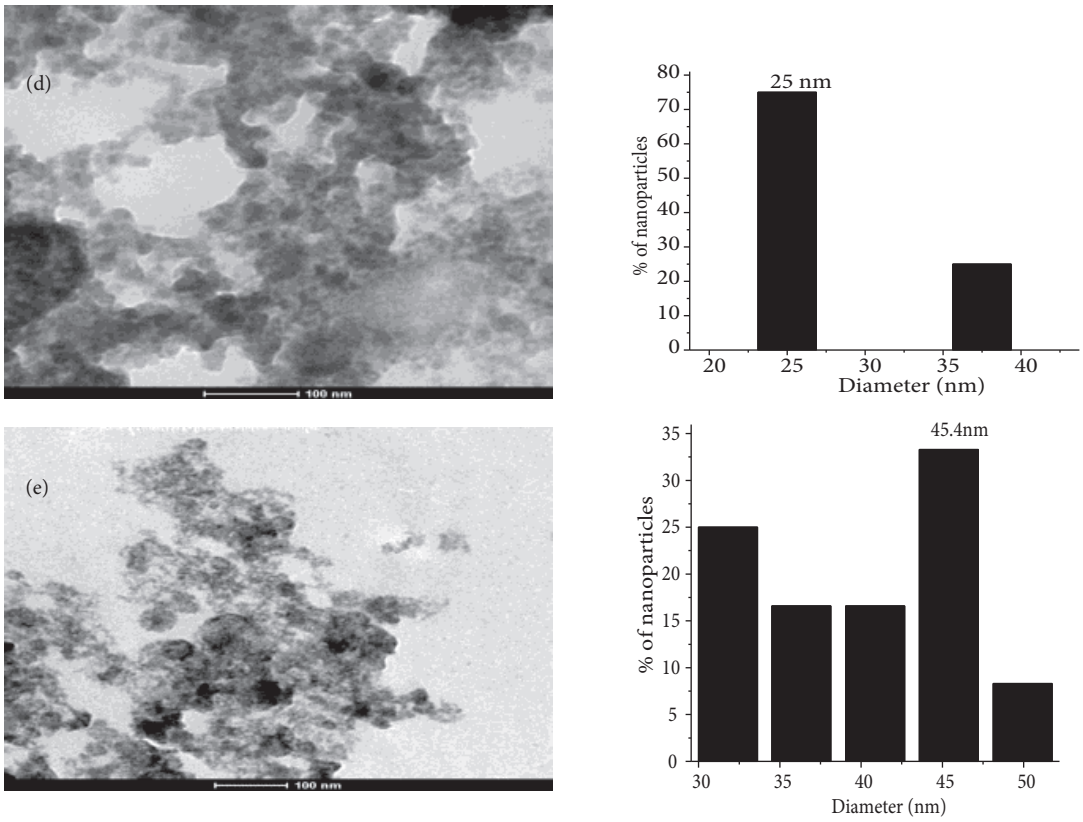

Figure 7. Continued.

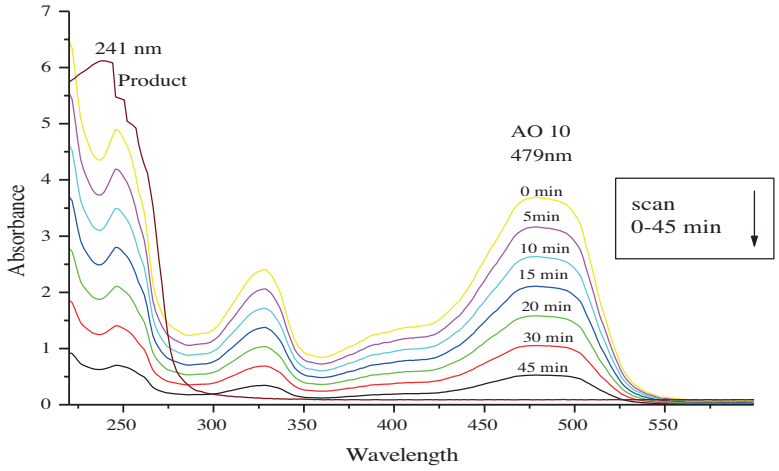

Figure 8. UV-vis spectra showing the degradation of AO 10.

2.7. Calculation of turnover frequencies

The turnover frequency (TOF), a term borrowed from enzyme catalysis, quantifies the specific activity of a catalytic center for a special reaction under defined reaction conditions by the number of molecules n reacted at each available catalytic site per unit time t.[16] Therefore, TOF has been calculated using the following

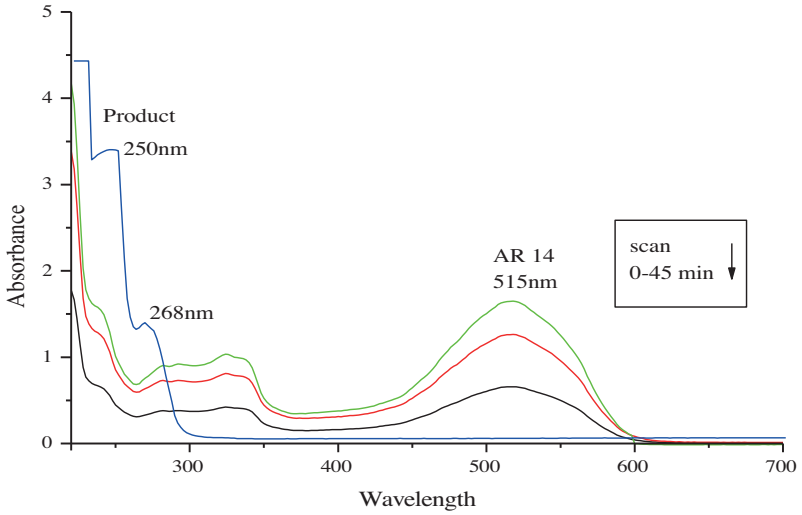

Figure 9. UV-vis spectra showing the degradation of AR 14.

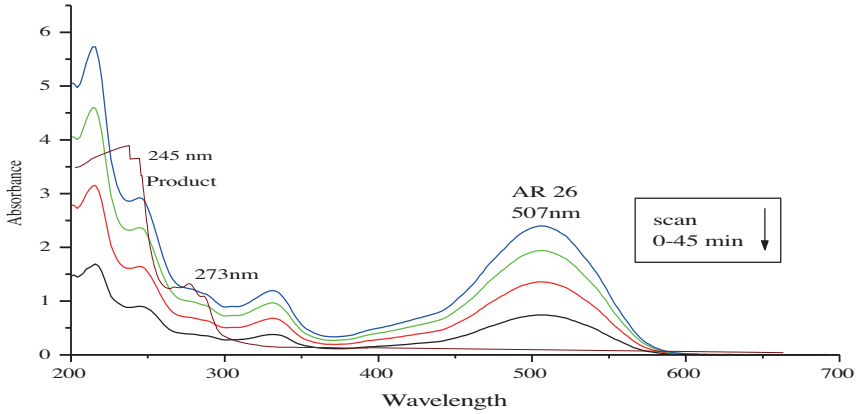

Figure 10. UV-vis spectra showing the degradation of AR 26.

Table 3. Calculation of turnover frequencies (TOF).

S. no.	Dyes under investigation	Approximate particle size (nm)		TOF (s^{-1})	
		PVP-IrO_2-nano	POLE-IrO_2-nano	PVP-IrO_2-nano	POLE-IrO_2-nano
1.	Acid orange 10	4.05 ± 0.25	21.21 ± 1.3	5.48	2.56
2.	Acid red 14	4.05 ± 0.25	21.21 ± 1.3	3.19	1.02
3.	Acid red 26	4.05 ± 0.25	21.21 ± 1.3	6.38	3.18

formula:

$$TOF = (1/N_{act})dn/dt,$$

where N_{act} is the number of active sites.

Assuming all surface atoms to be active, then $N_{act} = A_p/A_{UC}n$, where A_p is the surface area of the average particle size, A_{UC} is the surface area of an Ir unit cell face, and n is the number of Ir atoms in a unit

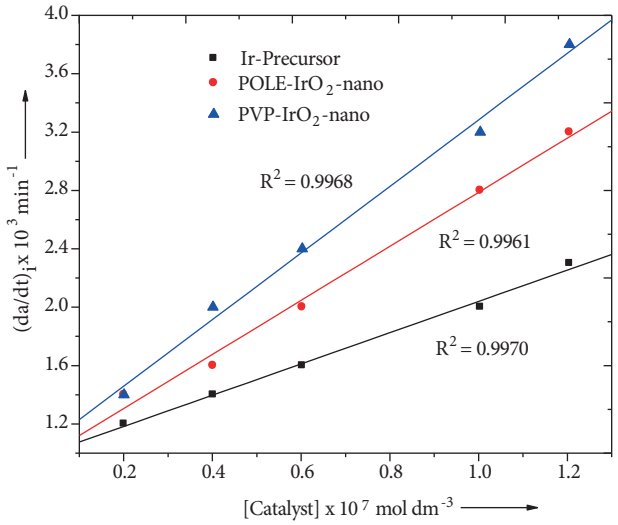

Figure 11. Plots between rate vs. concentration of catalyst for the oxidation of AO 10.

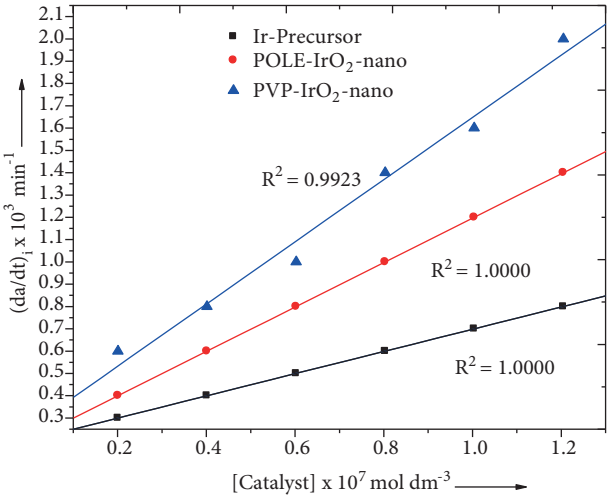

Figure 12. Plots between rate vs. concentration of catalyst for the oxidation of AR 14.

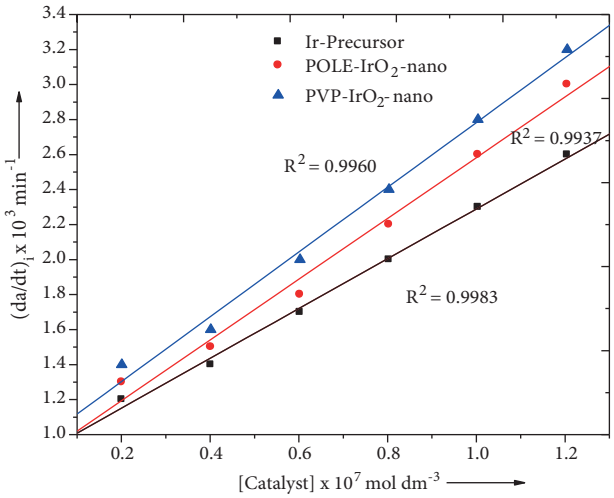

Figure 13. Plots between rate vs. concentration of catalyst for the oxidation of AR 26.

Table 4. Calculated values of k_1.

	Ir precursor catalyzed reaction	POLE-IrO_2-nano catalyzed reaction	PVP-IrO_2 nano catalyzed reaction
Acid orange 10	5.37×10^{-5} s^{-1}	7.37×10^{-5} s^{-1}	9.97×10^{-5} s^{-1}
Acid red 14	1.91×10^{-5} s^{-1}	3.07×10^{-5} s^{-1}	4.22×10^{-5} s^{-1}
Acid red 26	6.90×10^{-5} s^{-1}	8.44×10^{-5} s^{-1}	10.74×10^{-5} s^{-1}

cell face. Although only a small portion of surface Ir atoms can actually act as catalytically active sites, as many will be bonded to capping ligands and unavailable for catalysis, in practice, it is common to take the total number of surface atoms as the number of catalytic sites when the value is not known. The calculated values of TOF are presented in Table 3 for the oxidation of AO 10, AR 14, and AR 26, respectively.

2.8. Mechanism of degradation of azo dyes

The most probable mechanism for catalytic degradation of azo dyes by HCF(III) in the presence of IrO_2 nanoclusters can be illustrated as follows:

$$D^- + Ir_n \underset{k_{-1}}{\overset{k_1}{\rightleftharpoons}} \text{Complex}(C) \tag{1}$$

$$C + Fe(CN)_6^{3-} \xrightarrow[slow]{k_2} Ir_n + Fe(CN)_6^{4-} + \text{Products} \tag{2}$$

The experimental results and previous evidence[17] lead us to propose a mechanism for the above electron transfer reaction that involves the binding of a substrate to the surface of IrO_2 nanoclusters (Ir_n) and then reaction with HCF(III) ions present in solution. It is assumed that azo dyes exist as anions, D^-, in the alkaline medium, which form a loosely bonded complex with IrO_2 nanoclusters (Ir_n). This complex slowly reacts with HCF(III) ions, resulting in products along with Ir_n and $Fe(CN)_6^{4-}$. The proposed degradation pathways for AO 10, AR 14, and AR 26 are given in Schemes 1–3, respectively.

2.9. Conclusions

In this paper, a simple chemical method using methanol as a reducing agent and PVP and POLE as stabilizing agents for the synthesis of IrO_2 nanoclusters has been developed. IrO_2 nanoclusters were characterized by UV-vis, XRD, FT-IR, and TEM methods of analysis. From XRD and TEM images, it is evident that PVP-stabilized IrO_2 nanoclusters are amorphous and smaller in size with a narrow size distribution as compared to POLE-stabilized nanoparticles. The size of POLE-stabilized particles ranges from 16.45 to 43.12 nm, which is quite large in contrast to the size of PVP-stabilized IrO_2 nanoclusters (4.12 nm to 5.86 nm). Moreover, the sizes of synthesized IrO_2 nanoclusters can be tuned by varying the ratios of precursor to surfactant and solvent to reductant. Synthesized IrO_2 nanoclusters were employed for oxidative degradation of azo dyes, AO 10, AR 14, and AR 26. The reaction was found to follow first-order kinetics with regard to the concentration of IrO_2 nanoclusters. The comparison of the catalytic activity of Ir-Precursor, POLE-Ir-nano, and PVP-Ir-nano on the rate of oxidation of investigated dyes reveals the highest catalytic activity of PVP-IrO_2 nanoclusters. The IrO_2 nanoparticles are expected to be suitable alternatives and play an imperative role in the fields of catalysis and environmental remediation.

3. Experimental

3.1. Materials

Iridium trichloride ($IrCl_3.xH_2O$), purchased from Loba Chemie Pvt. Ltd., Mumbai, India, was used as a precursor. Polyvinylpyrrolidone (PVP), mean molecular weight 40,000, and polyoxyethylene(23) lauryl ether (POLE or Brij-35), mean molecular weight 1199, were obtained from Merck and Thomas Baker, respectively, and were used as stabilizing agents, while methanol procured from Merck was used as a reducing agent. The azo dye acid orange 10 was procured from Sisco Research Laboratories Pvt. Ltd., India, while acid red 14 and acid red 26 were purchased from Loba Chemie. All other reagents used were of analytical grade. Double-distilled water was used throughout the study.

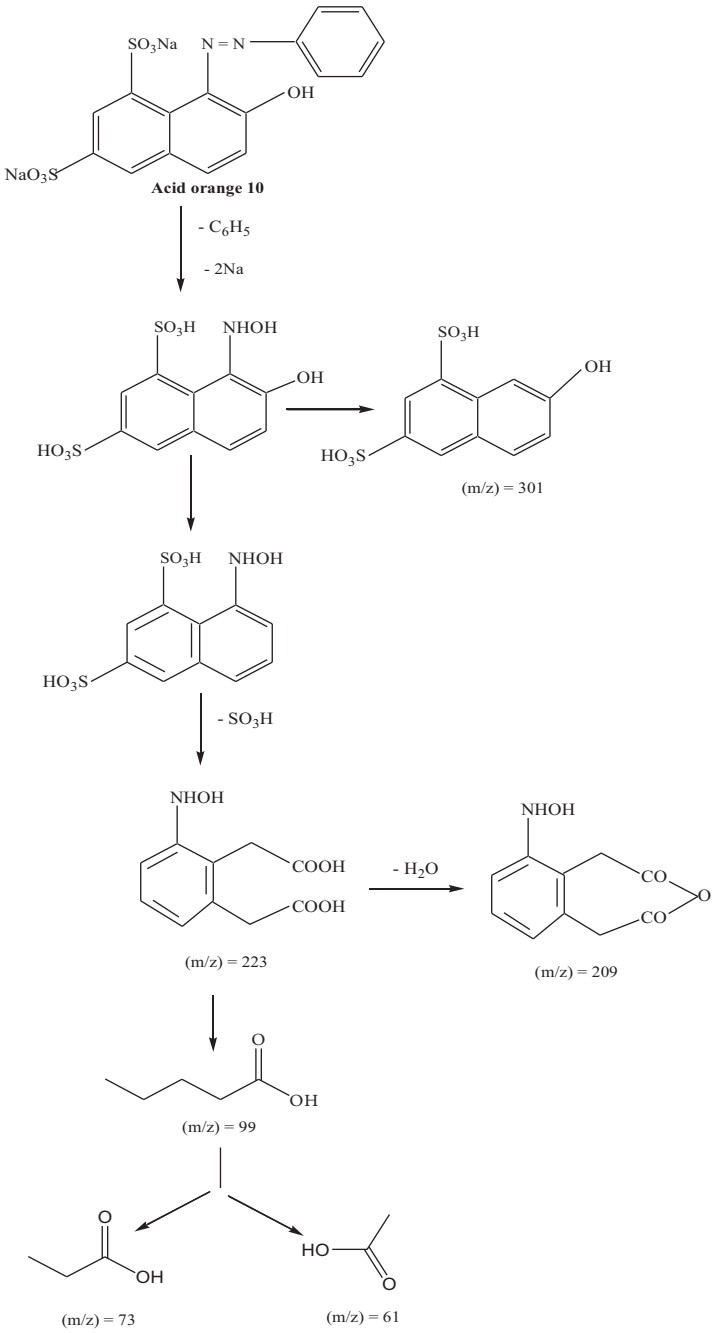

Scheme 1. Tentative degradation pathway for acid orange 10.

3.2. Synthesis of IrO_2 nanoclusters

In the present work the synthesis of IrO_2 nanoclusters by chemical reduction method as reported earlier by Goel et al.[18] using $IrCl_3.xH_2O$ precursor has been carried out. In order to prepare stable metal nanoclusters with a defined particle size and narrow size distribution, methanol as a reducing agent and PVP and POLE as stabilizers for controlling the metal particle size have been used. Series of experiments were carried out to show the effect of experimental conditions on the size of Ir nanoparticles. Calculated amounts of precursor ($IrCl_3.xH_2O$) and

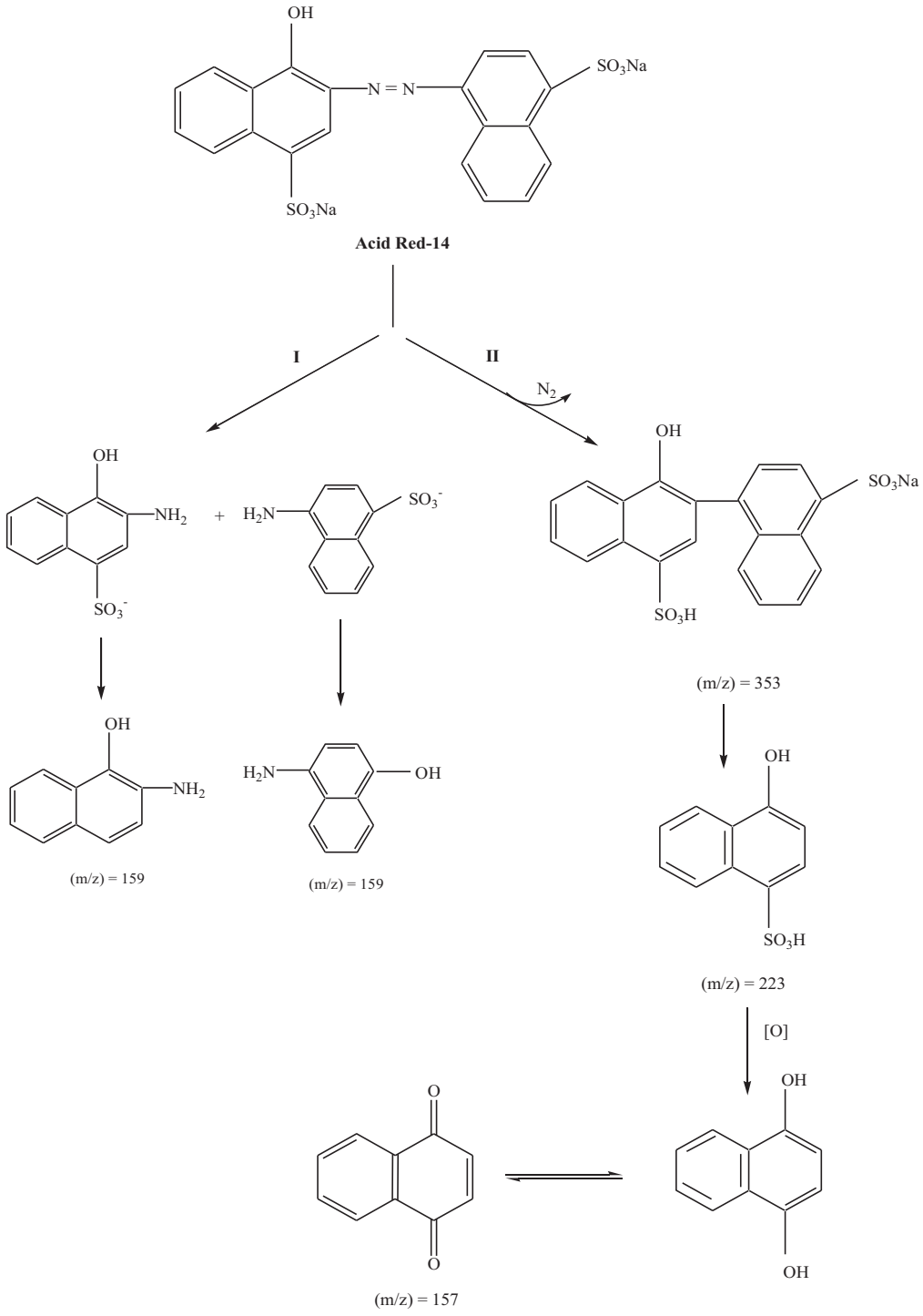

Scheme 2. Tentative degradation pathway for acid red 14.

stabilizer (PVP/POLE) were dissolved in a methanol-water mixed solvent at room temperature by stirring magnetically. An aqueous solution of sodium hydroxide (0.2 M) was added dropwise to the solution with vigorous stirring for 15 min. Then the solution was allowed to stir for a further 15 min on the same magnetic stirrer. After that, the solution was refluxed in an oil bath for 2 h. PVP/POLE-stabilized colloidal nanoparticles

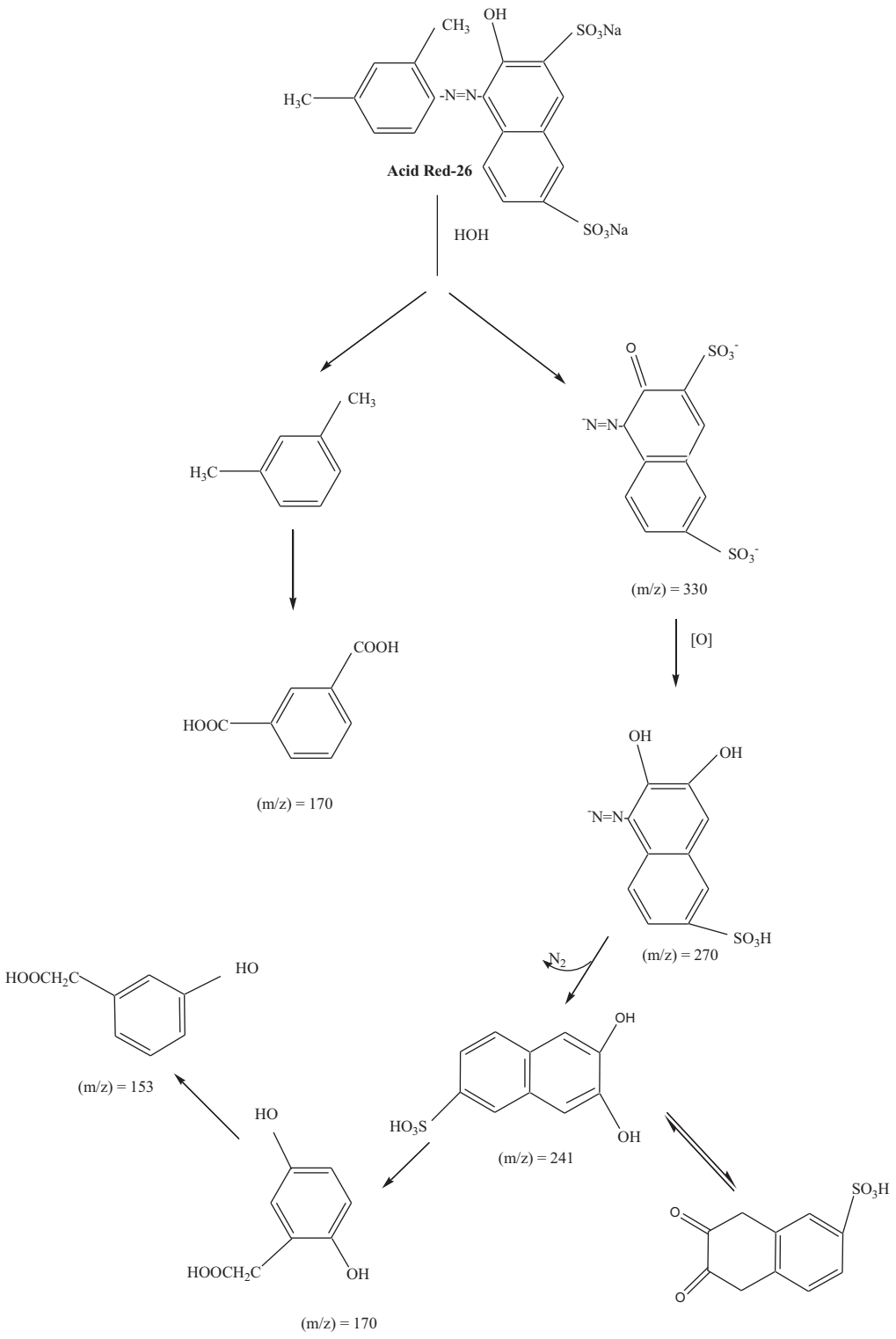

Scheme 3. Tentative degradation pathway for acid red 26.

were obtained. During the course of preparation of colloidal iridium nanoparticles, a succession of color changes in the reaction solution were observed (Scheme 4).

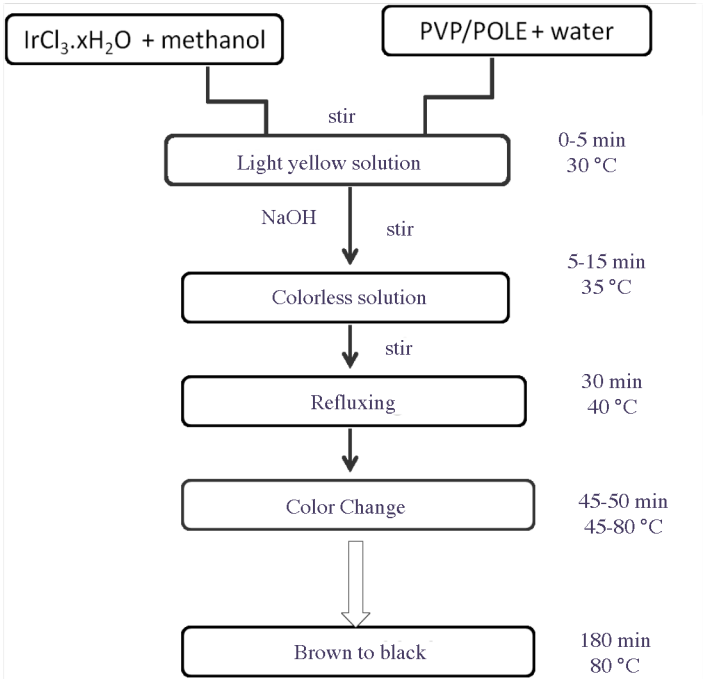

Scheme 4. The course of preparation of colloidal iridium nanoparticles.

The change in color from yellow to blackish-brown supports the formation of IrO_2 nanoclusters. By refluxing the reaction mixture for about 2 h, a transparent IrO_2 colloidal dispersion was obtained without precipitation. The resultant IrO_2 colloids were found to be stable for at least 6 months. Temperature changes during the synthesis are represented by Figure 14. The rise in temperature from 30 °C to 80 °C is observed, which tends to become constant after the formation of IrO_2 nanoclusters.

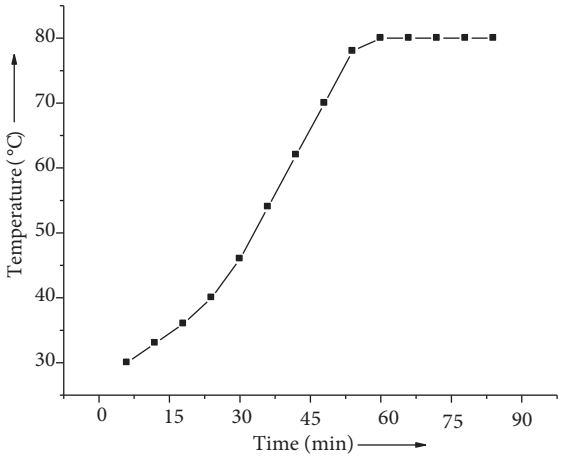

Figure 14. Time–temperature profile during the synthesis of IrO_2 nanoclusters.

Size-controlled synthesis of IrO_2 nanoclusters was carried out by varying the amount of stabilizer and reductant as described in Tables 1 and 2.

3.3. Characterization of IrO_2 nanoclusters

IrO_2 nanoclusters were characterized by XRD performed on the dry powders using a Bruker AXS D-8 Advance diffractometer with a scan rate of 1° min^{-1} and a Cu K_α X-ray source ($\lambda = 0.154$ nm). The size and morphology were determined by TEM (FEI-TECHNAI G-20). The infrared spectra were recorded in a wavenumber range of 800-4000 cm^{-1} by using a Bruker Alpha E-FTIR. UV-visible absorption spectra of synthesized IrO_2 nanoclusters were recorded on a Systronics UV-vis 117 spectrophotometer equipped with a 1-cm quartz cell.

3.4. Catalytic activity of synthesized IrO_2 nanoclusters

The catalytic activity of synthesized IrO_2 nanoclusters was evaluated by the oxidative degradation of azo dyes AO 10, AR 14, and AR 26 by HCF(III) using IrO_2 nanoclusters as a catalyst at constant temperature and pH. A reaction mixture containing 3.0×10^{-6} mol dm^{-3} HCF(III) and 1.004×10^{-7} mol dm^{-3} IrO_2 nanoclusters and a dye sample (3.0×10^{-5} mol dm^{-3}) were thermostated separately at 40 °C to attain thermal equilibrium. The pH of the reaction mixture was maintained by KH_2PO_4 and NaOH using a digital pH meter (Systronics μ pH System 361). The reaction was initiated by injecting the solution of dye into the aforementioned reaction mixture (prepared solution of HCF(III) and Ir-nano). Samples were withdrawn from the reaction mixture at preset time intervals using a pipette and were analyzed immediately. The progress of the reaction was measured spectrophotometrically (Systronics 117) with a spectrometric quartz cell (1 cm in path length) at the λ_{max} of the reaction mixture. As the reaction proceeds, the absorbance of the reaction mixture decreases with time. According to the Beer–Lambert law, the absorbance of dye is directly proportional to its concentration:

$$A = ecl,$$

where e is the molar absorption coefficient and l is the thickness of the absorption cell. Since the molar absorption coefficient (e) and thickness of the cell (l) are constant, the decrease in the absorbance of the reaction mixture with time shows a linear relationship between dye concentration and absorbance. The initial rate method was used to determine the kinetic behavior of these reactions. The initial reaction rate $(da/dt)_i$ for each set was calculated from the slope of the individual graph plotted between the values of absorbance at corresponding times using the plane mirror method.

References

1. Zhang, H.; Jin, M.; Xiong, Y.; Lim, B.; Xia, Y. *Acc. Chem. Res.* **2013**, *46*, 1783-1794.
2. Anjum, M.; Miandad, R.; Waqas, M.; Gehany, F.; Barakat, M. A. *Arab. J. Chem.* **2016** (in press).
3. Gupta, V. K.; Agarwal, S.; Saleh, T. A. *J. Hazard. Mater.* **2011**, *185*, 17-23.
4. Saleh, T. A.; Gupta, V. K. *Environ. Sci. Pollut. Res.* **2012**, *19*, 1224-1228.
5. Xia, X.; Figueroa-Cosme, L.; Tao, J.; Peng, H.; Niu, G.; Zhu, Y.; Xia, Y. *J. Am. Chem. Soc.* **2014**, *136*, 10878-10881.
6. Kundu, S.; Liang, H. *J. Colloid Interface Sci.* **2011**, *354*, 597-609.
7. Kant, R. *Natural Science* **2012**, *4*, 22-26.
8. Mondall, P.; Baksi, S.; Bos, D. *World Scientific News* **2017**, *61*, 98-109.
9. Khairy, M.; Zakaria, W. *Egyptian Journal of Petroleum* **2014**, *23*, 419-426.
10. Saikia, P.; Miah, A. T.; Das, P. P. *J. Chem. Sci.* **2017**, *129*, 81-93.
11. Goel, A.; Sharma, S. *International Transactions in Applied Science* **2009**, *12*, 243-251.

12. Malina, D.; Sobczak-Kupiec, A.; Wzorek, Z.; Kowalski Z. *Digest Journal of Nanomaterials and Biostructures* **2012**, *7*, 1527-1534.

13. Alahmad A. *Int. J. ChemTech Res.* **2014**, *6*, 450-459.

14. Goel, A.; Rani, N. *Open Journal of Inorganic Chemistry* **2012**, *2*, 67-73.

15. Ghasemi, S.; Rahimnejad, S.; Setayesh, S.; Rohani, S.; Gholami, M. R. *J. Hazard. Mater.* **2009**, *172*, 1573-1578.

16. Goel, A.; Lasyal, R. *Water Sci. Technol.* **2016**, *74*, 2551-2559.

17. Goel, A.; Lasyal, R. *Desalin. Water Treat.* **2016**, *57*, 17547-17556.

18. Goel, A.; Bhatt, R.; Neetu. *International Journal of Research in Chemistry and Environment* **2012**, *2*, 210-217.